SCIENCE CHINA
Physics, Mechanics & Astronomy

Few-layer metasurfaces with arbitrary scattering properties

Zhancheng Li, Wenwei Liu, Hua Cheng and Shuqi Chen

Citation: SCIENCE CHINA Physics, Mechanics & Astronomy **63**, 284202 (2020); doi: 10.1007/s11433-020-1583-3

View online: http://engine.scichina.com/doi/10.1007/s11433-020-1583-3

View Table of Contents: http://engine.scichina.com/publisher/scp/journal/SCPMA/63/8

Published by the Science China Press

SCIENCE CHINA
Physics, Mechanics & Astronomy

•Invited Review•
Special Topic: Metasurfaces of Novel Designs and Functionalities

August 2020 Vol. 63 No. 8: 284202
https://doi.org/10.1007/s11433-020-1583-3

Few-layer metasurfaces with arbitrary scattering properties

Zhancheng Li[1], Wenwei Liu[1], Hua Cheng[1*], and Shuqi Chen[1,2,3*]

[1] *The Key Laboratory of Weak Light Nonlinear Photonics, Ministry of Education, School of Physics and TEDA Institute of Applied Physics, Renewable Energy Conversion and Storage Center, Nankai University, Tianjin 300071, China;*
[2] *The Collaborative Innovation Center of Extreme Optics, Shanxi University, Taiyuan 030006, China;*
[3] *Collaborative Innovation Center of Light Manipulations and Applications, Shandong Normal University, Jinan 250358, China*

Received February 29, 2020; accepted May 25, 2020; published online June 22, 2020

Metasurfaces, which are planar arrays of subwavelength artificial structures, have emerged as excellent platforms for the integration and miniaturization of electromagnetic devices and provided ample possibilities for single-dimensional and multi-dimensional manipulations of electromagnetic waves. However, owing to the limited interactions between planar thin metallic nanostructures and electromagnetic waves as well as intrinsic losses in metals, metasurfaces exhibit disadvantages in terms of efficiency, controllability, and functionality. Recent advances in this field show that few-layer metasurfaces can overcome these drawbacks. Few-layer metasurfaces composed of more than one functional layer enable more degrees of design freedom. Hence, they possess unprecedented capabilities for electromagnetic wave manipulation, which have considerable impact in the area of nanophotonics. This article reviews recent advances in few-layer metasurfaces from the viewpoint of their scattering properties. The scattering matrix theory is briefly introduced, and the advantages and drawbacks of few-layer metasurfaces for the realization of arbitrary scattering properties are discussed. Then, a detailed overview of typical few-layer metasurfaces with various scattering properties and their design principles is provided. Finally, an outlook on the future directions and challenges in this promising research area is presented.

few-layer metasurfaces, light-matter interaction, scattering matrix, full-space manipulation

PACS number(s): 73.21.Ac, 78.20.Bh, 11.30.-j, 42.25.-p, 78.67.-n

Citation: Z. Li, W. Liu, H. Cheng, and S. Chen, Few-layer metasurfaces with arbitrary scattering properties, Sci. China-Phys. Mech. Astron. **63**, 284202 (2020), https://doi.org/10.1007/s11433-020-1583-3

1 Introduction

Arbitrary manipulation of electromagnetic waves is a fundamental requirement to realize electromagnetic devices with on-demand functionalities [1-4]. However, the limited light-matter interactions in natural materials hinder their efficient manipulation of electromagnetic waves [5-7]. Metasurfaces, which are planar arrays composed of subwavelength artificial structures, have recently emerged as excellent platforms for single-dimensional and multi-dimensional manipulations of electromagnetic waves, and they also provide a powerful alternative for the integration and miniaturization of electromagnetic devices [8-13]. By judiciously modulating the structural parameters of each unit cell, we can efficiently design the electromagnetic responses of metasurfaces at the subwavelength scale and implement electromagnetic functionalities on demand [14-16]. Owing to their prominent capabilities in electromagnetic wave manipulation, metasurfaces have been widely utilized in many fields, such as wave-front manipulation, beam focusing, imaging, sensing, optical encryption, and hologram [17-

*Corresponding authors (Hua Cheng, email: hcheng@nankai.edu.cn; Shuqi Chen, email: schen@nankai.edu.cn)

20]. However, despite their remarkable success, metasurfaces present some shortcomings in the arbitrary manipulation of electromagnetic waves. In the early designs, the constituent materials of metasurfaces were mainly metals, such as gold, silver, and aluminum [21-23]. The limited light-matter interactions between thin metallic nanostructures and electromagnetic waves as well as the intrinsic losses in metals are responsible for the low efficiency of metasurfaces and their limited controllability of electromagnetic waves [24-26]. Moreover, planar metasurfaces have limited degrees of design freedom for structural symmetry, which also limits their controllability and functionality [27].

Lossless dielectric materials have been widely utilized as the constituent materials of metasurfaces to significantly improve their efficiencies. Recent advances in dielectric metasurfaces indicate that metasurfaces constituted by lossless materials can help realize manipulation of electromagnetic waves with ultra-high efficiency [28-33]. Moreover, with the modulation of both the waveguide mode and resonance phase in dielectric nanostructures, the controllability of metasurfaces on the phase and amplitude of electromagnetic waves has improved significantly [34-36]. Even though metasurfaces constituted by dielectric materials can overcome some drawbacks in the existing metallic designs, the limited degrees of design freedom for structural symmetry still limit their performance, preventing the asymmetric and full-space manipulations of electromagnetic waves. Recently, few-layer metasurfaces composed of more than one functional layer have emerged as another powerful alternative for improving the efficiency, controllability, and functionality of metasurfaces [37]. With many interlayer interactions, the efficiency of few-layer metasurfaces can be improved significantly [38]. More importantly, the structural symmetry of few-layer metasurfaces can be arbitrarily designed, providing unprecedented capabilities for the asymmetric and full-space manipulation of electromagnetic waves. Few-layer metasurfaces with various scattering properties are currently garnering considerable interest from the scientific community. Owing to their unprecedented flexibility for the implementation of various electromagnetic functionalities, few-layer metasurfaces have been shown crucial in many applications [37-42].

We herein review the recent advances in few-layer metasurfaces from the viewpoint of their scattering properties. Sect. 2 introduces the scattering matrix theory as well as the advantages and drawbacks of few-layer metasurfaces for the realization of arbitrary scattering properties. In sect. 3, we present some typical few-layer metasurfaces with high efficiency and discuss their design principles. Subsequently, we present several exciting few-layer metasurfaces with special scattering properties in sect. 4. Finally, we provide an outlook on the further directions and challenges in this promising research area.

2 Scattering properties of metasurfaces

2.1 Scattering matrix theory

The scattering matrix, which involves transmission and reflection operators in both forward and backward directions, relates the inputs and outputs at the two edges of an electromagnetic system composed of plane parallel layers, as shown in Figure 1(a) [43]. It is often used to describe transmission lines, microwave circuits, and scattering systems. In this case, the outgoing fields can be expressed in terms of the incident fields as follows:

$$\begin{bmatrix}\mathbf{E}_2^{\text{out}}\\ \mathbf{E}_1^{\text{out}}\end{bmatrix}=\mathbf{S}\begin{bmatrix}\mathbf{E}_1^{\text{in}}\\ \mathbf{E}_2^{\text{in}}\end{bmatrix}=\begin{bmatrix}\mathbf{t}_{21} & \mathbf{r}_{22}\\ \mathbf{r}_{11} & \mathbf{t}_{12}\end{bmatrix}\begin{bmatrix}\mathbf{E}_1^{\text{in}}\\ \mathbf{E}_2^{\text{in}}\end{bmatrix}, \tag{1}$$

where the elements of the **S** matrix are expressed as $\mathbf{t}_{21}$, $\mathbf{r}_{22}$, $\mathbf{r}_{11}$, and $\mathbf{t}_{12}$. $\mathbf{t}_{21}$ and $\mathbf{r}_{11}$ are the matrices of the transmission and reflection coefficients in the forward direction, respectively; $\mathbf{t}_{12}$ and $\mathbf{r}_{22}$ are the matrices of the transmission and reflection coefficients in the backward direction, respectively. Specifically, considering that the basis polarization vectors of the incident and outgoing fields are linear-polarized in the *x*- and *y*-directions, we can further express eq. (1) as follows:

$$\begin{bmatrix}E_{2x}^{\text{out}}\\ E_{2y}^{\text{out}}\\ E_{1x}^{\text{out}}\\ E_{1y}^{\text{out}}\end{bmatrix}=\mathbf{S}\begin{bmatrix}E_{1x}^{\text{in}}\\ E_{1y}^{\text{in}}\\ E_{2x}^{\text{in}}\\ E_{2y}^{\text{in}}\end{bmatrix}=\begin{bmatrix}t_{21}^{xx} & t_{21}^{xy} & r_{22}^{xx} & r_{22}^{xy}\\ t_{21}^{yx} & t_{21}^{yy} & r_{22}^{yx} & r_{22}^{yy}\\ r_{11}^{xx} & r_{11}^{xy} & t_{12}^{xx} & t_{12}^{xy}\\ r_{11}^{yx} & r_{11}^{yy} & t_{12}^{yx} & t_{12}^{yy}\end{bmatrix}\begin{bmatrix}E_{1x}^{\text{in}}\\ E_{1y}^{\text{in}}\\ E_{2x}^{\text{in}}\\ E_{2y}^{\text{in}}\end{bmatrix}. \tag{2}$$

If the system is lossless, the incident and outgoing optical power values must be equal. In this case, the energy conservation dictates that

$$\left(t_{21}^{xx}\right)^2+\left(t_{21}^{yx}\right)^2+\left(r_{11}^{xx}\right)^2+\left(r_{11}^{yx}\right)^2=1, \tag{3a}$$

$$\left(t_{21}^{xy}\right)^2+\left(t_{21}^{yy}\right)^2+\left(r_{11}^{xy}\right)^2+\left(r_{11}^{yy}\right)^2=1, \tag{3b}$$

$$\left(r_{22}^{xx}\right)^2+\left(r_{22}^{yx}\right)^2+\left(t_{12}^{xx}\right)^2+\left(t_{12}^{yx}\right)^2=1, \tag{3c}$$

$$\left(r_{22}^{xy}\right)^2+\left(r_{22}^{yy}\right)^2+\left(t_{12}^{xy}\right)^2+\left(t_{12}^{yy}\right)^2=1. \tag{3d}$$

Moreover, the coefficients of the scattering matrix for a metasurface are not mutually independent [26]. For example, for a system with time inversion symmetry, the reciprocity theorem can be applied, and the transmission coefficients in the forward and backward directions can be correlated as follows:

$$\mathbf{t}_{12}=\begin{bmatrix}t_{12}^{xx} & t_{12}^{xy}\\ t_{12}^{yx} & t_{12}^{yy}\end{bmatrix}=\begin{bmatrix}t_{21}^{xx} & t_{21}^{yx}\\ t_{21}^{xy} & t_{21}^{yy}\end{bmatrix}. \tag{4}$$

This relationship differs from that in the Jones matrix be-

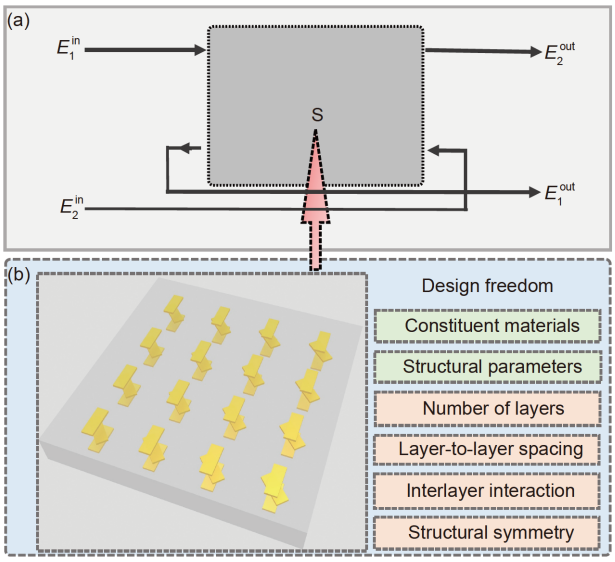

Figure 1 (Color online) Advantages of few-layer metasurfaces for the realization of arbitrary scattering properties. (a) Mathematical description of scattering matrix **S** that relates the inputs and outputs of electromagnetic waves based on transmission and reflection operators in two opposite directions. (b) Schematics of a typical tri-layer metasurface and degrees of design freedom of few-layer metasurfaces for electromagnetic wave manipulation.

cause no coordinate transformation is involved. In addition, the relationships between the coefficients of the scattering matrix in a metasurface are related to the structural symmetry. For example, for a metasurface whose structure is C_4-symmetric with respect to the axis perpendicular to the surface, the transmission coefficients can be correlated as follows:

$$\mathbf{t}_{21}=\begin{bmatrix} t_{21}^{xx} & t_{21}^{xy} \\ t_{21}^{yx} & t_{21}^{yy} \end{bmatrix}=\begin{bmatrix} t_{21}^{xx} & t_{21}^{xy} \\ -t_{21}^{xy} & t_{21}^{xx} \end{bmatrix}. \tag{5}$$

The coefficients of the scattering matrix in a metasurface depend on many variables, such as the k vector of the incident waves, wavelength of the incident waves, and time. As the scattering properties of each unit cell in a metasurface can be independently manipulated, the coefficients of the scattering matrix in a metasurface depend on the spatial position of each unit cell as well.

2.2 Metasurfaces with different scattering properties

Metasurfaces with different electromagnetic responses and functionalities are mainly implemented by manipulating their scattering properties, i.e., by adjusting one or more coefficients of their scattering matrices. For example, metasurfaces with $\mathbf{t}_{21}$ and $\mathbf{r}_{11}$ equal to zero in multiple or broadband wavelengths can realize perfect absorption of the electromagnetic waves in the forward direction [44-46]. As another example, in a metasurface whose structure is mirror symmetric with respect to the plane perpendicular to its surface, the cross-polarized transmission coefficients t_{21}^{xy} and t_{21}^{yx} can be equal to zero. Hence, the polarization manipulation of electromagnetic waves can be obtained by adjusting the real and imaginary parts of the co-polarized transmission coefficients t_{21}^{xx} and t_{21}^{yy} [47-49]. By setting the co-polarized transmission coefficients $t_{21}^{xx}=0$ and cross-polarized transmission coefficients $t_{21}^{yx}\neq 0$, the cross-polarization conversion can be obtained [50]. One specific scattering property of metasurfaces is asymmetric transmission. According to eq. (4), the transmission intensities for the forward and backward illuminations with a fixed polarization state differ when the amplitudes of the cross-polarized transmission coefficients t_{21}^{xy} and t_{21}^{yx} are not equal to each other. However, the asymmetric transmissions of linear-polarized electromagnetic waves cannot be realized because the planar structures of the metasurfaces are mirror symmetric with respect to the surface. Nonetheless, the asymmetric transmission of circular-polarized electromagnetic waves can be realized, which only requires the nonzero sum of the cross-polarized transmission coefficients [51-55].

By independently adjusting one or more coefficients of the scattering matrix of each unit cell, metasurfaces can exhibit more functionalities [16]. For example, the phase manipulations of electromagnetic waves at the subwavelength scale can be realized by independently adjusting the cross-polarized transmission coefficients of each unit cell; this has been widely utilized to manipulate the electromagnetic wavefront and has broad applications in optical focusing, computer-generated holograms, vectors, vortex beam generation, etc. [54-59]. In addition, metasurfaces can integrate different electromagnetic functionalities or display different electromagnetic responses under different illumination conditions by adjustment of one or more coefficients of their scattering matrices at different wavelengths or incident angles [60-64]. In general, by controlling their scattering properties, metasurfaces are excellent for the effective manipulation of electromagnetic waves. However, as mentioned above, the drawbacks in the working efficiency and design freedom of structural symmetry of metasurfaces prevent them from the asymmetric and full-space manipulation of electromagnetic waves with high efficiency.

2.3 Advantages and drawbacks of few-layer designs

Compared with single-layer metasurfaces, few-layer metasurfaces contain more available degrees of design freedom, as shown in Figure 1(b). Not only can the constituent materials and the structural parameters be adjusted, but also some key physical parameters, such as the number of layers, layer-to-layer spacing, interlayer interactions, and structural symmetry can be designed when configuring the few-layer metasurfaces. Utilizing the abundant interlayer interactions,

such as the near-field coupling effect, the waveguide effect, and the multiple wave interference effect, the efficiency of few-layer metasurfaces can be improved significantly [38]. By manipulating the number of layers and the layer-to-layer spacing, the scattering properties of few-layer metasurfaces can be further adjusted. Furthermore, the structural symmetry of few-layer metasurfaces can be arbitrarily designed and therefore the coefficients of their scattering matrices can be independently adjusted, promising the asymmetric and full-space manipulation of electromagnetic waves with high efficiency.

The multiple degrees of design freedom in few-layer metasurfaces may involve some complexities. More degrees of design freedom imply a more complicated and time-consuming optimization process. The selection of number of layers and constituent materials of each layer, and the optimization of layer-to-layer spacing and nanostructure configuration of each layer will significantly increase the design complexity. The increase in the number of layers will result in enhanced light-matter interactions in few-layer metasurfaces, which further improves the working efficiency. However, the number of layers should not be excessive as the enhanced light-matter interactions increase the Ohmic losses. In some situations, owing to the complex near-field interactions between the layers, the electromagnetic response of each layer in a few-layer metasurface is associated with the alignment and distance between the layers, which further complicates the optimization processes. Few-layer metasurfaces typically have high fabrication requirements, e.g., a strict alignment between layers is required for the fabrication of few-layer metasurfaces with near-field interactions between the layers. Despite some complexities induced during the design and optimization process, the few-layer metasurface is still a suitable and powerful platform for the implementation of arbitrary scattering properties by utilizing some appropriate optimization processes [38].

Next, we present the unprecedented capacities of few-layer metasurfaces for the realization of arbitrary scattering properties by reviewing some exciting achievements in this research area.

3 Few-layer metasurfaces with high efficiencies

In most cases, light-matter interactions within metallic metasurfaces involve only electric responses, which results in limited efficiency [65-68]. For example, the amplitudes of cross-polarized transmission coefficients do not exceed 0.5 in the metallic metasurfaces [68]. In few-layer metasurfaces, not only the electric response, but also the magnetic response can be involved by utilizing the abundant interlayer interactions to significantly improve the efficiency [38,65]. Multiple wave interference within layers is one of the main interlayer interactions in few-layer metallic metasurfaces, which has been used to efficiently manipulate electromagnetic waves in the reflection mode through metal-insulator-metal designs [69-74]. The multiple wave interference effect can also be utilized in the transmission mode to enhance light-matter interactions within few-layer metasurfaces. The few-layer metasurface containing a Fabry-Pérot-like cavity is an early configuration to enhance the amplitudes of cross-polarized transmission coefficients in the transmission mode, as shown in Figure 2(a) [75]. The Fabry-Pérot-like cavity is composed of two orthogonal gold gratings. One of them can transmit y-polarized electromagnetic waves, whereas the other one can transmit x-polarized electromagnetic waves. The main function of the Fabry-Pérot-like cavity is to enhance the interaction between the nanostructures in the middle layer and the electromagnetic waves. As shown in Figure 2(b), the proposed few-layer metallic metasurface serves as a broadband linear polarization converter in the transmission mode with over 0.5 efficiency. The co-polarized transmittance and the cross-polarized reflectance are practically zero when using the gratings. By independently adjusting the cross-polarized transmission coefficients of each unit cell, we can further achieve a high-efficiency manipulation of the electromagnetic waves' wavefront, as shown in Figure 2(c) and (d). Currently, this configuration is a popular design to achieve high-performance linear polarization converters [76-78].

As the scattering matrix of a few-layer system can be obtained from the scattering properties of each layer when the near-field interactions between the layers are negligible, the Fabry-Pérot-like cavity is not a necessary component for the design of few-layer metallic metasurfaces with high efficiency [79-82]. Figure 3(a) shows a tri-layer metasurface that can be used to realize giant asymmetric transmission of the circular-polarized optical waves at a wavelength of 1.5 μm [83]. Compared with previous approaches, the performance of the asymmetric transmission in the proposed tri-layer metasurface improved significantly with a 20:1 extinction ratio and over 50% transmittance in one of the circular-polarized optical waves, as shown in Figure 3(b). The giant asymmetric transmission of the circular-polarized optical waves in this tri-layer metasurface is achieved by independently designing the electric admittances of each layer, and the scattering properties of the tri-layer metasurface can be presented in terms of the cascaded layer admittances. This is a good alternative method for the design of few-layer metasurfaces [82-84]. The few-layer metasurfaces discussed above can enhance the amplitude of the cross-polarized transmission coefficients in their scattering matrices while minimizing the amplitude of the co-polarized transmission coefficients. In fact, the amplitude of the co-polarized transmission coefficients can be improved in few-layer metasurfaces. Figure 3(c) shows a bilayer aluminum metasur-

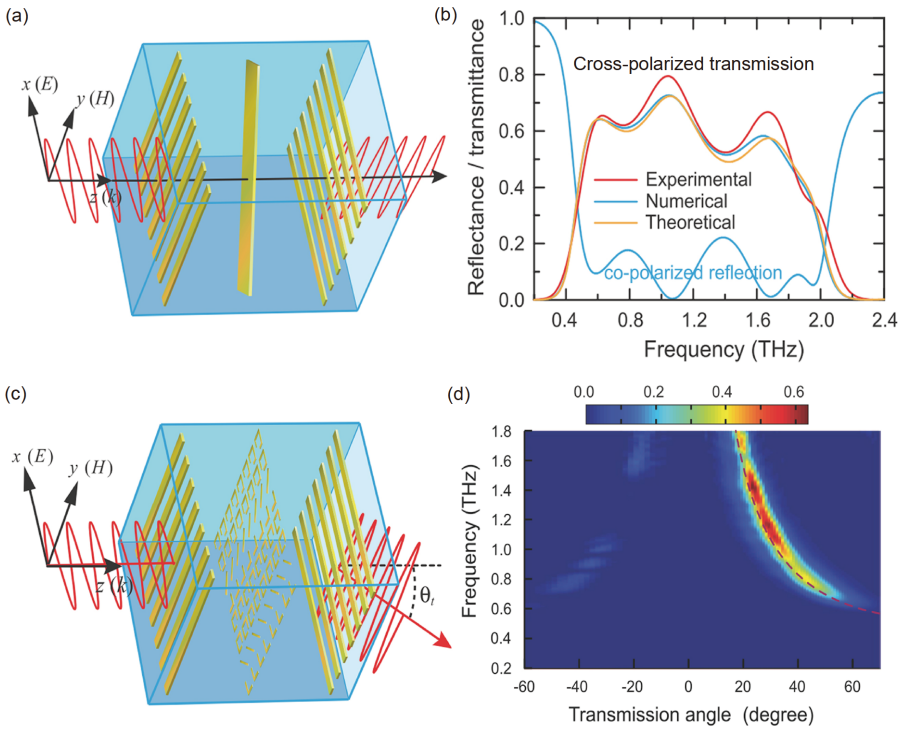

Figure 2 (Color online) Few-layer metasurfaces based on Fabry-Pérot-like cavity. (a) Schematic of a tri-layer metasurface for the realization of a linear polarization converter with high efficiency. (b) Experimentally measured, numerically simulated, and theoretically calculated results of cross-polarized transmittance, and numerically simulated result of co-polarized reflectance. (c) Schematic of a tri-layer metasurface for broadband and high-efficiency anomalous refraction. (d) Experimental results of cross-polarized transmittance as a function of frequency and angle. (a)-(d) reproduced with permission from ref. [75], copyright 2013, American Association for the Advancement of Science.

face that can be treated as a broadband linear polarizer in the near infrared regime (as shown in Figure 3(d)) [85]. In this design, the modular square of the co-polarized transmission coefficient t_{21}^{yy} is approximately 0.89 from 1050 to 1350 nm, whereas those of transmission coefficients t_{21}^{xx}, t_{21}^{xy}, and t_{21}^{yx} are equal to zero. Compared with the single layer metasurface, the proposed bilayer metasurface has a broad working bandwidth and a high extinction ratio, as shown in Figure 3(e). Thehigh performance of the proposed bilayer design is attributed to the multiple wave interference between the layers, and the scattering properties of this bilayer metasurface can be predicated by the scattering matrix of each layer. A number of few-layer metasurfaces based on the scattering matrix theory have been proposed to manipulate electromagnetic waves with high efficiency [86-93].

For few-layer designs based on the scattering matrix theory, the scattering properties can be manipulated by designing the scattering matrix of each layer. Moreover, their scattering properties can be further adjusted by changing the layer-to-layer spacing and number of layers [75,82]. Figure 4(a) and (b) show a bilayer metasurface whose cross-polarized transmission coefficient t_{21}^{yx} can be continuously manipulated by varying the distance between the two layers [94]. The nanoantenna array in the bilayer metasurface can almost completely reflect the *x*-polarized optical waves in the working waveband that will interfere with the incident *x*-polarized optical waves, resulting in the change in the electric field distribution above the nanoantenna array, as shown in Figure 4(b). Furthermore, the L-shape particle can be regarded as a polarization converter, whose efficiency is directly associated with the magnitude of the electric field within it. Hence, the polarization conversion efficiency of the bilayer metasurface can be changed by varying the distance between the L-shaped particle and the nanoantenna array. Figure 4(c) and (d) show a narrow band-pass filter composed of few-layer nanostructures, whose bandwidth and efficiency can be manipulated by changing the number of layers [95]. The scattering property of this filter can be fully described by the multiple wave interference theory. Another typical approach is a few-layer metasurface composed of stacked nanorods, in which the transmission efficiency of left-handed circular-polarized (LCP) waves decreases with the increasing number of layers, whereas that of the right-handed circular-polarized (RCP) waves increases accordingly [96].

In general, few-layer metasurfaces are known to be important for the manipulation of electromagnetic waves with high efficiency and afford more degrees of design freedom.

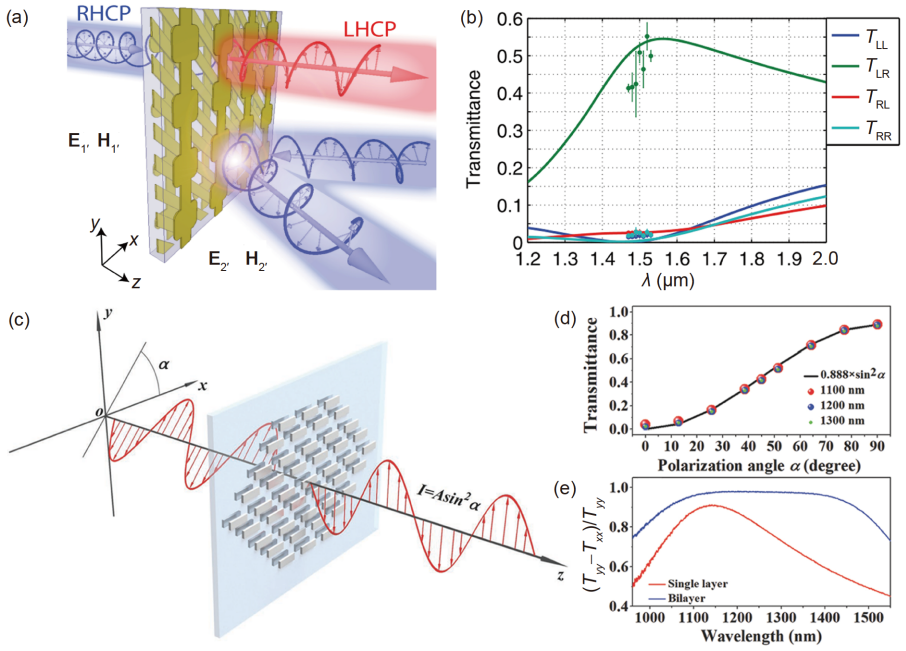

Figure 3 (Color online) Few-layer metasurface supported by scattering matrix theory. (a) Schematic of a high-performance bianisotropic tri-layer metasurface for the realization of the giant asymmetric transmission of circular-polarized optical waves. (b) Experimentally measured (circles) and numerically simulated (solid lines) results of squared moduli of transmission coefficients under a circular base. (c) Schematic of a bilayer metasurface for broadband polarization extinction. (d) Experimentally measured transmittance as a function of polarization angle α of the linear-polarized illumination at 1100, 1200, and 1300 nm. (e) Comparison of transmission extinction ratio between metasurfaces with a single layer and a bilayer of nanorods. (a), (b) Reproduced with permission from ref. [83], copyright 2014, American Physical Society. (c)-(e) Reproduced with permission from ref. [85], copyright 2019, Wiley-VCH.

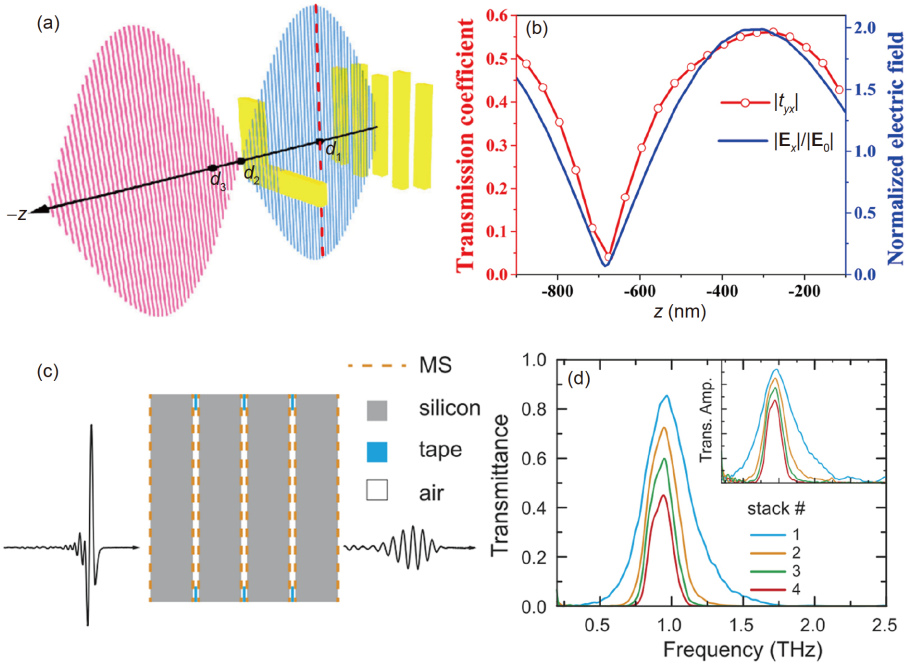

Figure 4 (Color online) Manipulation of scattering properties of few-layer metasurfaces by changing layer-to-layer spacing and number of layers. (a) Schematic of a unit cell of a bilayer metasurface composed of an L-shaped particle and a nanoantenna array. (b) Simulated results of *x*-component distribution of electric field along *z*-axis, and variation in the absolute value of the transmission coefficient t_{yx} in the forward direction with the change in the position of the L-shaped particle. (c) Schematic of a few-layer metasurface composed of multiple bilayer structures. (d) Measured transmittance of few-layer metasurfaces with different stack assemblies. (a), (b) Reproduced with permission from ref. [94], copyright 2015, Springer Nature. (c), (d) Reproduced under the terms of the CC-BY Creative Commons Attribution 4.0 International License (http://creativecommons.org/licenses/by/4.0/) [95], copyright 2018, the Authors, published by American Institute of Physics.

4 Few-layer metasurfaces with special scattering properties

As mentioned above, the key feature of few-layer metasurfaces is that their structural symmetry can be arbitrarily designed to form some scattering properties that cannot be achieved by single-layer metasurfaces. Figure 5(a) shows a bilayer metasurface in which the asymmetric transmission of linear-polarized optical waves was first obtained [97]. The proposed bilayer metasurface with three dimensional and nonsymmetrical designs can achieve the asymmetric transmission of both circular- and linear-polarized optical waves as its transmission coefficients are not equal to each other, as shown in Figure 5(b) and (c). Moreover, the asymmetric transmission of linear-polarized electromagnetic waves can be further realized by appropriately adjusting the transmission coefficients of the scattering matrix, whereas the transmittance is symmetric for circular-polarized electromagnetic waves [98]. Furthermore, the cross-polarized and co-polarized transmission coefficients can be set to zero and then a diode-like unidirectional transmission of electromagnetic waves can be achieved, as shown in Figure 5(d)-(f) [99]. In the proposed bilayer metasurface, the modular square of the cross-polarized transmission coefficient t_{21}^{yx} and the co-polarized transmission coefficient t_{21}^{xx} are approximately zero, whereas the modular square of the cross-polarized transmission coefficient t_{21}^{xy} remains constant from 1150 to 1450 nm, which results in a diode-like unidirectional transmission of linear-polarized optical waves. The realization of asymmetric transmission and diode-like unidirectional transmission of linear-polarized electromagnetic waves is a popular topic in the research area of few-layer metasurfaces [100-104]. Apart from the asymmetric transmission of linear-polarized electromagnetic waves, few-layer metasurfaces possess other special scattering properties as well. Figure 5(g) shows a pair of bilayer metasurfaces that can be used to realize the spin-selective transmission of circular-polarized optical waves [105]. The structural mirror symmetry in these two metasurfaces is broken by the bilayer

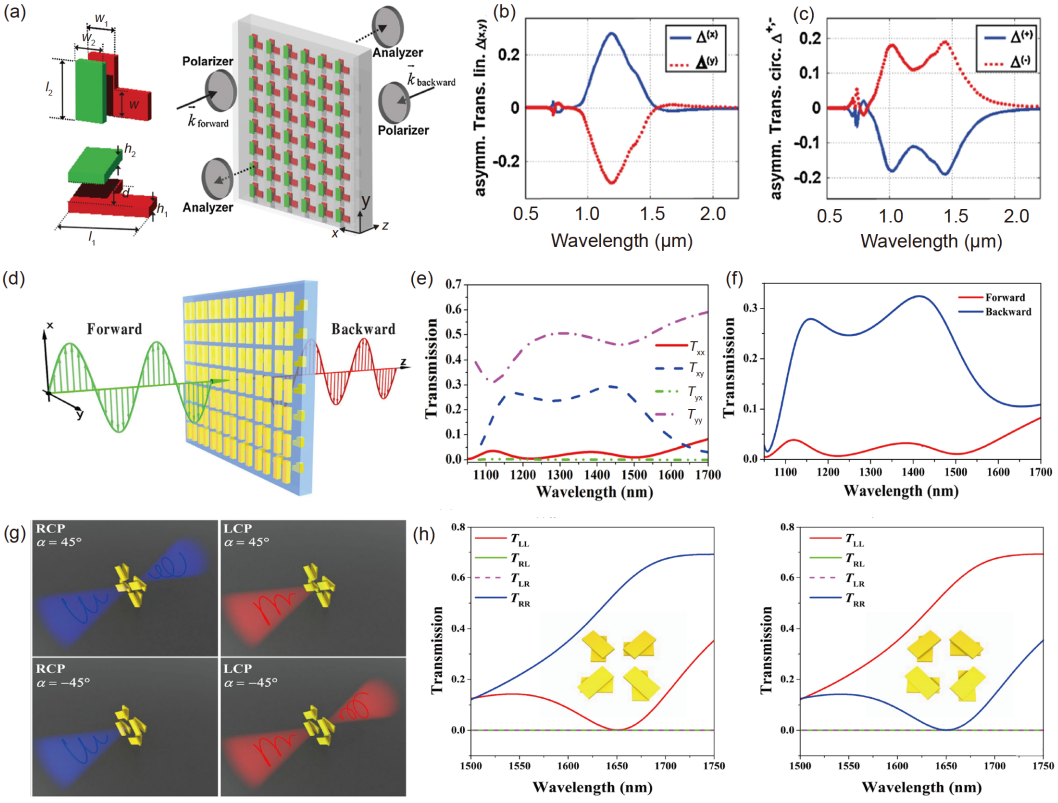

Figure 5 (Color online) Manipulation of scattering properties of few-layer metasurfaces based on special structural symmetry design. (a) Schematic of a bilayer metasurface for the realization of asymmetric transmission of linear-polarized optical waves, and schematic of the experimental setup. Numerically simulated results of the asymmetric transmission for (b) linear and (c) circular states. (d) Schematic of a bilayer metasurface for the realization of broadband diode-like asymmetric transmission of linear-polarized optical waves. (e) Numerically simulated results of squared moduli of transmission coefficients under forward illumination. (f) Simulated results of transmission spectra for *x*-polarized waves propagating along forward and backward directions. (g) Schematic of a pair of bilayer metasurfaces for the realization of spin-selective transmission of LCP and RCP waves, respectively. (h) Simulated results of squared moduli of transmission coefficients under a circular base for the proposed bilayer metasurfaces (unit cell as shown in the inset image). (a)-(c) Reproduced with permission from ref. [97], copyright 2010, American Physical Society. (d)-(f) Reproduced with permission from ref. [99], copyright 2014, American Institute of Physics. (g), (h) Reproduced under the terms of the CC-BY Creative Commons Attribution 4.0 International License (http://creativecommons.org/licenses/by/4.0/) [105], copyright 2017, the Authors, published by Springer Nature.

design, whereas their structure is C_4-symmetric with respect to the axis perpendicular to their surfaces. This special design of structural symmetry results in the zero amplitudes of the cross-polarized transmission coefficients (under circular base) t_{21}^{lr} and t_{21}^{rl}. Moreover, the amplitude of one of the co-polarized transmission coefficients can be adjusted to zero because they can be independently manipulated in this design. Owing to this specific design of the transmission coefficients, the spin-selective transmission of optical waves canbe observed in the proposed bilayer metasurfaces, as shown in Figure 5(h). By breaking the structural mirror symmetry in the few-layer metasurfaces, other chiral optical responses can be obtained [106-109]. Recently, the unidirectional reflection of electromagnetic waves, which is associated with the conception of exceptional point and cannot be achieved in single-layer metasurfaces, has been widely investigated in few-layer metasurfaces [110-113]. In these designs, the reflection coefficients of their scattering matrices in one propagation direction are equal to zero at the working wavelength, resulting in the unidirectional reflection of electromagnetic waves. From the abovementioned progress, it is clear that few-layer metasurfaces with abundant and different scattering properties can be utilized to efficiently manipulate electromagnetic waves.

More importantly, the scattering properties of each unit cell in a few-layer metasurface can be independently manipulated, which provide unprecedented possibilities for the asymmetric and full-space manipulation of electromagnetic waves. Figure 6(a) shows a bilayer metasurface in which not only the diode-like unidirectional transmission of linear-polarized optical waves, but also the subwavelength phase manipulation of transmission waves can be realized [114]. This design is similar to the abovementioned design [99], which involves the subwavelength phase manipulation of transmission waves by changing the structural parameters of the L-shaped particle in each unit cell. Using this design, the asymmetric polarization encryption based on holograms can be obtained, as shown in Figure 6(b). Figure 6(c) shows a tri-layer metasurface that can realize the asymmetric wavefront manipulation of circular-polarized optical waves (as shown in Figure 6(d)) [115]. The scattering matrix of this tri-layer metasurface was specially designed, in which only four cross-polarized coefficients are not equal to zero at the working waveband, resulting in the diode-like unidirectional transmission of circular-polarized optical waves. Furthermore, the asymmetric wavefront manipulation in this tri-layer design was achieved by utilizing the geometric phase. In addition to the asymmetric manipulation of electromagnetic waves, few-layer metasurfaces have been proposed to realize the full-space manipulation of electro-magnetic waves in some recent studies [116-122]. As shown in Figure 7(a), most previous designs of metasurfaces only function in either transmission or reflection mode, leaving half of the electromagnetic space unutilized [116]. Even if the asymmetric manipulation of electromagnetic waves can be realized through the abovementioned few-layer designs, the independent phase manipulation of transmission and reflection waves are still not realizable [115]. Recent advances in few-layer metasurfaces have overcome these drawbacks. By independently designing multiple coeffi-

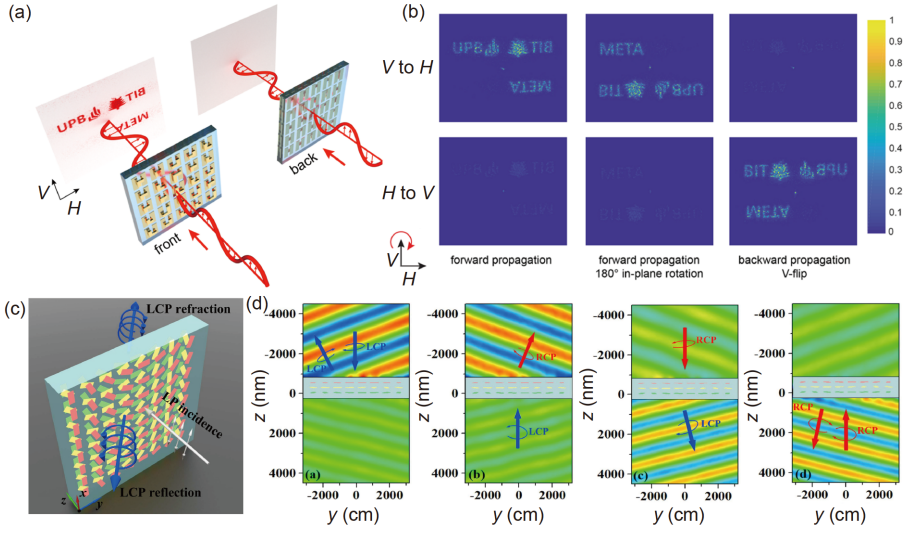

Figure 6 (Color online) Asymmetric scattering properties in few-layer metasurfaces. (a) Illustration of asymmetric functionality of a bilayer metasurface. (b) Measured holograms under different illumination directions and polarization states. (c) Schematic of a tri-layer metasurface for the realization of asymmetric anomalous refraction and reflection. (d) Time snapshot of amplitude distribution of electric field under LCP/RCP forward and backward illuminations. (a), (b) Reproduced with permission from ref. [114], copyright 2019, American Chemical Society. (c), (d) Reproduced under the terms of the CC-BY Creative Commons Attribution 4.0 International License (http://creativecommons.org/licenses/by/4.0/) [115], copyright 2016, the Authors, published by Springer Nature.

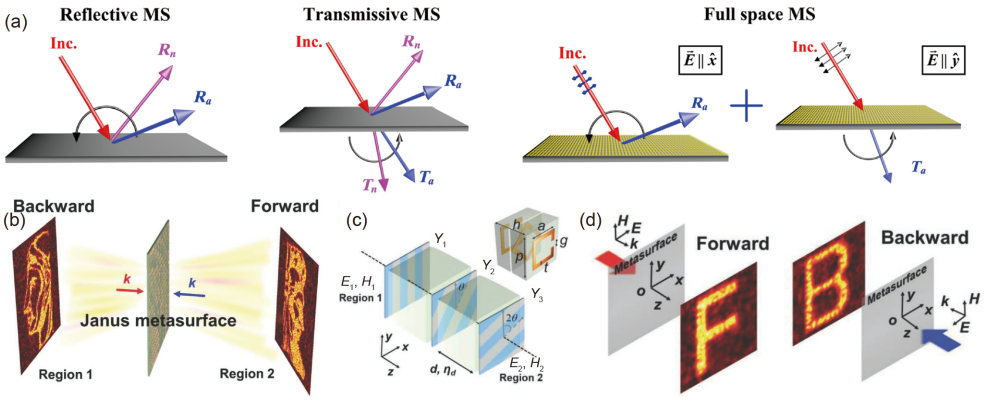

Figure 7 (Color online) Full-space manipulation of electromagnetic waves based on few-layer metasurfaces. (a) Working principle and advantages of the full-space metasurfaces. (b) Illustration of the Janus tri-layer metasurface. (c) Schematics of theoretical model and twisted tri-layer meta-atom. (d) Calculated results of transmitted electric field distribution under forward and backward illuminations. (a) Reproduced with permission from ref. [116], copyright 2017, American Physical Society. (b)-(d) Reproduced with permission from ref. [122], copyright 2020, Wiley-VCH.

cients of their scattering matrices, the few-layer metasurfaces, whose electromagnetic responses are dependent on both the incident direction and the polarization state of the incident waves, can realize the full-space manipulation of electromagnetic waves and the integration of multiple electromagnetic functionalities [116-121]. For example, three different functionalities can be integrated into a few-layer metasurface by independently designing the reflection coefficients r_{11}^{xx} and r_{22}^{xx}, and the transmission coefficient t_{21}^{yy} [117]. A recent approach further demonstrated that the full-space manipulation of electromagnetic waves can be achieved by the interleaved design of few-layer metasurfaces, as shown in Figure 7(b) [122]. The basic unit cell of this design is shown in Figure 7(c), which is designed based on the scattering matrix theory. This basic unit cell can realize the unidirectional transmission of electromagnetic waves with phase control. By applying a 90° rotation in the plane, the rotated unit cell can achieve the unidirectional transmission of electromagnetic waves in the opposite direction. Furthermore, by arranging these two types of unit cells in an interleaved manner, i.e., a 90° twisted angle between two neighboring unit cells, distinct directional holograms can be obtained, as shown in Figure 7(d).

In general, few-layer metasurfaces are an excellent candidate to realize special scattering properties, and they offer unprecedented possibilities for the asymmetric and full-space manipulation of electromagnetic waves.

5 Conclusions

We presented the recent advances in few-layer metasurfaces in terms of their scattering properties. Owing to their abundant interlayer interactions and more degrees of design freedom, few-layer metasurfaces are excellent platforms for the efficient manipulation of electromagnetic waves, and provide unprecedented possibilities for the asymmetric and full-space manipulation of electromagnetic waves and the integration of multiple electromagnetic functionalities. Currently, few-layer metasurfaces with special scattering properties are garnering more attention from the scientific community. We herein proposed several promising directions in this research field that may benefit nanophotonics significantly.

The relationship between the design freedom of few-layer metasurfaces and their scattering matrices is indispensable for the implementation of few-layer metasurfaces with scattering properties on demand. Recently, the interplays between the number of layers and phase coverage in few-layer metasurfaces have been well discussed [123]. This type of study will considerably simplify the design process of few-layer metasurfaces, which also benefits the realization of specific electromagnetic functionalities in few-layer metasurfaces.

By designing different constituent materials or different structures in each layer, few-layer metasurfaces have shown unprecedented flexibility for the integration of different electromagnetic functionalities. Recent approaches have proven the potential of few-layer metasurfaces as an alternative for the multispectral control of electromagnetic waves [124-126]. Meanwhile, the newly proposed dielectric few-layer metasurfaces have been proven to be a powerful platform for integrated photonics [127,128]. Hence, few-layer metasurfaces will be fundamental in achieving frequency-selective multifunctional electromagnetic devices and integrated devices.

The dynamic manipulation of the scattering properties of few-layer metasurfaces further provided a good platform for the manipulation and integration of multiple electromagnetic functionalities. A tunable polarization rotator based on a few-layer metasurface has been proposed recently based on the scattering matrix theory [129]. The dynamic manipula-

tion of the scattering properties of few-layer metasurfaces will further improve the controllability and functionality of few-layer metasurfaces.

The independent design of multiple coefficients of a scattering matrix was time consuming and complex owing to the plentiful degrees of design freedom in few-layer metasurfaces. The reversal design of few-layer metasurfaces using deep-learning technologies will overcome this drawback and ease the design of few-layer metasurfaces with specific scattering properties [130-132].

Benefitting from their scattering properties, which can be arbitrarily designed, few-layer metasurfaces indicated ample possibilities in various application areas. The comprehensive investigation of the application potentials of few-layer metasurfaces in nanophotonics has become a popular topic in this research area. For example, a recent work indicated that few-layer metasurfaces may be utilized to achieve neural computations [133].

This work was supported by the National Key Research and Development Program of China (Grant Nos. 2016YFA0301102, and 2017YFA0303800), the National Natural Science Fund for Distinguished Young Scholar (Grant No. 11925403), the National Natural Science Foundation of China (Grant Nos. 11974193, 11904181, 11904183, 91856101, and 11774186), the Natural Science Foundation of Tianjin for Distinguished Young Scientists (Grant No. 18JCJQJC45700), the National Postdoctoral Program for Innovative Talents (Grant No. BX20180148), and the China Postdoctoral Science Foundation (Grant Nos. 2018M640224, and 2018M640229).

1 N. I. Zheludev, Science **348**, 973 (2015).
2 J. Wang, Sci. China-Phys. Mech. Astron. **62**, 34201 (2019).
3 Q. H. Song, Sci. China-Phys. Mech. Astron. **62**, 074231 (2019).
4 L. K. Chen, and Y. F. Xiao, Sci. China-Phys. Mech. Astron. **63**, 224231 (2019).
5 Y. Liu, and X. Zhang, Chem. Soc. Rev. **40**, 2494 (2011).
6 N. I. Zheludev, and Y. S. Kivshar, Nat. Mater. **11**, 917 (2012).
7 A. Poddubny, I. Iorsh, P. Belov, and Y. Kivshar, Nat. Photon. **7**, 948 (2013).
8 X. G. Luo, Sci. China-Phys. Mech. Astron. **58**, 594201 (2015).
9 N. Meinzer, W. L. Barnes, and I. R. Hooper, Nat. Photon. **8**, 889 (2014).
10 S. Chen, Z. Li, W. Liu, H. Cheng, and J. Tian, Adv. Mater. **31**, 1802458 (2019).
11 S. Chen, W. Liu, Z. Li, H. Cheng, and J. Tian, Adv. Mater. **32**, 1805912 (2020).
12 W. Du, X. Wen, D. Gérard, C. W. Qiu, and Q. Xiong, Sci. China-Phys. Mech. Astron. **63**, 244201 (2020).
13 R. Y. Wu, L. Bao, L. W. Wu, and T. J. Cui, Sci. China-Phys. Mech. Astron. **63**, 284211 (2020).
14 H. H. Hsiao, C. H. Chu, and D. P. Tsai, Small Methods **1**, 1600064 (2017).
15 S. Chen, Z. Li, Y. Zhang, H. Cheng, and J. Tian, Adv. Opt. Mater. **6**, 1800104 (2018).
16 W. Liu, Z. Li, H. Cheng, S. Chen, and J. Tian, Phys. Rev. Appl. **8**, 014012 (2017).
17 X. Luo, Adv. Mater. **31**, 1804680 (2019).
18 D. Neshev, and I. Aharonovich, Light Sci. Appl. **7**, 58 (2018).
19 X. Luo, D. P. Tsai, M. Gu, and M. Hong, Adv. Opt. Photon. **10**, 757 (2018).
20 S. Sun, Q. He, J. Hao, S. Xiao, and L. Zhou, Adv. Opt. Photon. **11**, 380 (2019).
21 N. Liu, M. Mesch, T. Weiss, M. Hentschel, and H. Giessen, Nano Lett. **10**, 2342 (2010).
22 Y. Zhao, and A. Alù, Nano Lett. **13**, 1086 (2013).
23 Y. W. Huang, W. T. Chen, W. Y. Tsai, P. C. Wu, C. M. Wang, G. Sun, and D. P. Tsai, Nano Lett. **15**, 3122 (2015).
24 X. Ni, N. K. Emani, A. V. Kildishev, A. Boltasseva, and V. M. Shalaev, Science **335**, 427 (2012).
25 Z. Li, H. Cheng, Z. Liu, S. Chen, and J. Tian, Adv. Opt. Mater. **4**, 1230 (2016).
26 N. Yu, F. Aieta, P. Genevet, M. A. Kats, Z. Gaburro, and F. Capasso, Nano Lett. **12**, 6328 (2012).
27 C. Menzel, C. Rockstuhl, and F. Lederer, Phys. Rev. A **82**, 053811 (2010).
28 M. I. Shalaev, J. Sun, A. Tsukernik, A. Pandey, K. Nikolskiy, and N. M. Litchinitser, Nano Lett. **15**, 6261 (2015).
29 L. Wang, S. Kruk, H. Tang, T. Li, I. Kravchenko, D. N. Neshev, and Y. S. Kivshar, Optica **3**, 1504 (2016).
30 M. Khorasaninejad, W. T. Chen, A. Y. Zhu, J. Oh, R. C. Devlin, D. Rousso, and F. Capasso, Nano Lett. **16**, 4595 (2016).
31 H. Zuo, D. Y. Choi, X. Gai, P. Ma, L. Xu, D. N. Neshev, B. Zhang, and B. Luther-Davies, Adv. Opt. Mater. **5**, 1700585 (2017).
32 S. Gao, C. Park, S. Lee, and D. Choi, Adv. Opt. Mater. **7**, 1801337 (2019).
33 S. Gao, C. Park, C. Zhou, S. Lee, and D. Choi, Adv. Opt. Mater. **7**, 1900883 (2019).
34 J. P. B. Mueller, N. A. Rubin, R. C. Devlin, B. Groever, and F. Capasso, Phys. Rev. Lett. **118**, 113901 (2017).
35 W. Liu, Z. Li, H. Cheng, C. Tang, J. Li, S. Zhang, S. Chen, and J. Tian, Adv. Mater. **30**, 1706368 (2018).
36 W. Liu, Z. Li, Z. Li, H. Cheng, C. Tang, J. Li, S. Chen, and J. Tian, Adv. Mater. **31**, 1901729 (2019).
37 H. Cheng, Z. Liu, S. Chen, and J. Tian, Adv. Mater. **27**, 5410 (2015).
38 S. Chen, Y. Zhang, Z. Li, H. Cheng, and J. Tian, Adv. Opt. Mater. **7**, 1801477 (2019).
39 A. Epstein, J. P. S. Wong, and G. V. Eleftheriades, Nat. Commun. **7**, 10360 (2016).
40 W. L. Guo, K. Chen, G. M. Wang, X. Y. Luo, Y. J. Feng, and C. W. Qiu, IEEE Trans. Antennas Propagat. **68**, 1426 (2020).
41 K. Chen, Y. Feng, F. Monticone, J. Zhao, B. Zhu, T. Jiang, L. Zhang, Y. Kim, X. Ding, S. Zhang, A. Alù, and C. W. Qiu, Adv. Mater. **29**, 1606422 (2017).
42 K. Achouri, and C. Caloz, Nanophotonics **7**, 1095 (2018).
43 B. E. A. Saleh, and M. C. Teich, *Fundamentals of Photonics*, Ch. 7, (Wiley, Hoboken, 2007), pp. 246–279.
44 S. Chen, H. Cheng, H. Yang, J. Li, X. Duan, C. Gu, and J. Tian, Appl. Phys. Lett. **99**, 253104 (2011).
45 H. Cheng, S. Chen, H. Yang, J. Li, X. An, C. Gu, and J. Tian, J. Opt. **14**, 085102 (2012).
46 K. Fan, J. Y. Suen, X. Liu, and W. J. Padilla, Optica **4**, 601 (2017).
47 Z. Li, W. Liu, H. Cheng, S. Chen, and J. Tian, Sci. Rep. **5**, 18106 (2016).
48 T. Li, X. Hu, H. Chen, C. Zhao, Y. Xu, X. Wei, and G. Song, Opt. Express **25**, 23597 (2017).
49 Z. Ma, S. M. Hanham, Y. Gong, and M. Hong, Opt. Lett. **43**, 911 (2018).
50 W. Liu, S. Chen, Z. Li, H. Cheng, P. Yu, J. Li, and J. Tian, Opt. Lett. **40**, 3185 (2015).
51 Z. Li, W. Liu, H. Cheng, S. Chen, and J. Tian, Opt. Lett. **41**, 3142 (2016).
52 A. S. Schwanecke, V. A. Fedotov, V. V. Khardikov, S. L. Prosvirnin, Y. Chen, and N. I. Zheludev, Nano Lett. **8**, 2940 (2008).
53 R. Singh, E. Plum, C. Menzel, C. Rockstuhl, A. K. Azad, R. A. Cheville, F. Lederer, W. Zhang, and N. I. Zheludev, Phys. Rev. B **80**, 153104 (2009).
54 N. Yu, P. Genevet, M. A. Kats, F. Aieta, J. P. Tetienne, F. Capasso, and Z. Gaburro, Science **334**, 333 (2011).
55 E. Maguid, I. Yulevich, D. Veksler, V. Kleiner, M. L. Brongersma,

and E. Hasman, Science **352**, 1202 (2016).
56 F. Yue, D. Wen, J. Xin, B. D. Gerardot, J. Li, and X. Chen, ACS Photon. **3**, 1558 (2016).
57 G. Zheng, H. Mühlenbernd, M. Kenney, G. Li, T. Zentgraf, and S. Zhang, Nat. Nanotech. **10**, 308 (2015).
58 X. Chen, M. Chen, M. Q. Mehmood, D. Wen, F. Yue, C. W. Qiu, and S. Zhang, Adv. Opt. Mater. **3**, 1201 (2015).
59 Y. Zhang, W. Liu, J. Gao, and X. Yang, Adv. Opt. Mater. **6**, 1701228 (2018).
60 H. Cheng, X. Wei, P. Yu, Z. Li, Z. Liu, J. Li, S. Chen, and J. Tian, Appl. Phys. Lett. **110**, 171903 (2017).
61 X. Zhang, M. Pu, J. Jin, X. Li, P. Gao, X. Ma, C. Wang, and X. Luo, Annalen Der Phys. **529**, 1700248 (2017).
62 C. Zhang, F. Yue, D. Wen, M. Chen, Z. Zhang, W. Wang, and X. Chen, ACS Photon. **4**, 1906 (2017).
63 Y. Bao, Y. Yu, H. Xu, Q. Lin, Y. Wang, J. Li, Z. K. Zhou, and X. H. Wang, Adv. Funct. Mater. **28**, 1805306 (2018).
64 X. Wang, A. Díaz-Rubio, V. S. Asadchy, G. Ptitcyn, A. A. Generalov, J. Ala-Laurinaho, and S. A. Tretyakov, Phys. Rev. Lett. **121**, 256802 (2018).
65 A. Arbabi, and A. Faraon, Sci. Rep. **7**, 43722 (2017).
66 W. Luo, S. Sun, H. X. Xu, Q. He, and L. Zhou, Phys. Rev. Appl. **7**, 044033 (2017).
67 N. Papasimakis, V. A. Fedotov, V. Savinov, T. A. Raybould, and N. I. Zheludev, Nat. Mater. **15**, 263 (2016).
68 X. Ding, F. Monticone, K. Zhang, L. Zhang, D. Gao, S. N. Burokur, A. de Lustrac, Q. Wu, C. W. Qiu, and A. Alù, Adv. Mater. **27**, 1195 (2015).
69 H. T. Chen, Opt. Express **20**, 7165 (2012).
70 R. Fan, B. Xiong, R. Peng, and M. Wang, Adv. Mater. **32**, 1904646 (2019).
71 S. Sun, Q. He, S. Xiao, Q. Xu, X. Li, and L. Zhou, Nat. Mater. **11**, 426 (2012).
72 S. Sun, K. Y. Yang, C. M. Wang, T. K. Juan, W. T. Chen, C. Y. Liao, Q. He, S. Xiao, W. T. Kung, G. Y. Guo, L. Zhou, and D. P. Tsai, Nano Lett. **12**, 6223 (2012).
73 A. Pors, M. G. Nielsen, and S. I. Bozhevolnyi, Opt. Lett. **38**, 513 (2013).
74 S. C. Jiang, X. Xiong, Y. S. Hu, Y. H. Hu, G. B. Ma, R. W. Peng, C. Sun, and M. Wang, Phys. Rev. X **4**, 021026 (2014).
75 N. K. Grady, J. E. Heyes, D. R. Chowdhury, Y. Zeng, M. T. Reiten, A. K. Azad, A. J. Taylor, D. A. R. Dalvit, and H. T. Chen, Science **340**, 1304 (2013).
76 D. Y. Liu, M. H. Li, X. M. Zhai, L. F. Yao, and J. F. Dong, Opt. Express **22**, 11707 (2014).
77 H. Chen, H. Ma, J. Wang, S. Qu, Y. Pang, M. Yan, and Y. Li, Appl. Phys. A **122**, 463 (2016).
78 L. Cong, W. Cao, X. Zhang, Z. Tian, J. Gu, R. Singh, J. Han, and W. Zhang, Appl. Phys. Lett. **103**, 171107 (2013).
79 Y. Zhao, N. Engheta, and A. Alù, Metamaterials **5**, 90 (2011).
80 A. N. Askarpour, Y. Zhao, and A. Alù, Phys. Rev. B **90**, 054305 (2014).
81 L. Jing, Z. Wang, Y. Yang, L. Shen, B. Zheng, F. Gao, H. Wang, E. Li, and H. Chen, IEEE Trans. Antennas Propagat. **66**, 7148 (2018).
82 C. Pfeiffer, and A. Grbic, Phys. Rev. Appl. **2**, 044011 (2014).
83 C. Pfeiffer, C. Zhang, V. Ray, L. J. Guo, and A. Grbic, Phys. Rev. Lett. **113**, 023902 (2014).
84 C. Pfeiffer, C. Zhang, V. Ray, L. Jay Guo, and A. Grbic, Optica **3**, 427 (2016).
85 Z. Li, W. Liu, H. Cheng, D. Choi, S. Chen, and J. Tian, Adv. Opt. Mater. **7**, 1900260 (2019).
86 M. Jia, Z. Wang, H. Li, X. Wang, W. Luo, S. Sun, Y. Zhang, Q. He, and L. Zhou, Light Sci Appl **8**, 16 (2019).
87 S. Tang, T. Cai, J. G. Liang, Y. Xiao, C. W. Zhang, Q. Zhang, Z. Hu, and T. Jiang, Opt. Express **27**, 1816 (2019).
88 P. Yu, J. Li, C. Tang, H. Cheng, Z. Liu, Z. Li, Z. Liu, C. Gu, J. Li, S. Chen, and J. Tian, Light Sci Appl **5**, e16096 (2016).
89 J. Liu, Z. Li, W. Liu, H. Cheng, S. Chen, and J. Tian, Adv. Opt. Mater. **4**, 2028 (2016).
90 Z. H. Jiang, L. Kang, W. Hong, and D. H. Werner, Phys. Rev. Appl. **9**, 064009 (2018).
91 W. Ji, T. Cai, G. Wang, H. Li, C. Wang, H. Hou, and C. Zhang, Opt. Express **27**, 2844 (2019).
92 Z. H. Jiang, L. Kang, T. Yue, H. Xu, Y. Yang, Z. Jin, C. Yu, W. Hong, D. H. Werner, and C. Qiu, Adv. Mater. **32**, 1903983 (2020).
93 Y. Zhao, J. Shi, L. Sun, X. Li, and A. Alù, Adv. Mater. **26**, 1439 (2014).
94 Z. Li, S. Chen, W. Liu, H. Cheng, Z. Liu, J. Li, P. Yu, B. Xie, and J. Tian, Plasmonics **10**, 1703 (2015).
95 C. C. Chang, L. Huang, J. Nogan, and H. T. Chen, APL Photonics **3**, 051602 (2018).
96 Y. Zhao, M. A. Belkin, and A. Alù, Nat. Commun. **3**, 870 (2012).
97 C. Menzel, C. Helgert, C. Rockstuhl, E. B. Kley, A. Tünnermann, T. Pertsch, and F. Lederer, Phys. Rev. Lett. **104**, 253902 (2010).
98 M. Kang, J. Chen, H. X. Cui, Y. Li, and H. T. Wang, Opt. Express **19**, 8347 (2011).
99 Z. Li, S. Chen, C. Tang, W. Liu, H. Cheng, Z. Liu, J. Li, P. Yu, B. Xie, Z. Liu, J. Li, and J. Tian, Appl. Phys. Lett. **105**, 201103 (2014).
100 J. Han, H. Li, Y. Fan, Z. Wei, C. Wu, Y. Cao, X. Yu, F. Li, and Z. Wang, Appl. Phys. Lett. **98**, 151908 (2011).
101 C. Huang, Y. Feng, J. Zhao, Z. Wang, and T. Jiang, Phys. Rev. B **85**, 195131 (2012).
102 M. Mutlu, A. E. Akosman, A. E. Serebryannikov, and E. Ozbay, Phys. Rev. Lett. **108**, 213905 (2012).
103 J. H. Shi, H. F. Ma, C. Y. Guan, Z. P. Wang, and T. J. Cui, Phys. Rev. B **89**, 165128 (2014).
104 C. Zhang, C. Pfeiffer, T. Jang, V. Ray, M. Junda, P. Uprety, N. Podraza, A. Grbic, and L. J. Guo, Laser Photon. Rev. **10**, 791 (2016).
105 Z. Li, W. Liu, H. Cheng, S. Chen, and J. Tian, Sci. Rep. **7**, 8204 (2017).
106 Y. Cui, L. Kang, S. Lan, S. Rodrigues, and W. Cai, Nano Lett. **14**, 1021 (2014).
107 C. Huang, Y. Zhang, Y. Wang, and L. Kong, Phys. Rev. Appl. **10**, 064038 (2018).
108 M. Zhang, Q. Lu, and H. Zheng, J. Opt. Soc. Am. B **35**, 689 (2018).
109 M. A. Cole, W. Chen, M. Liu, S. S. Kruk, W. J. Padilla, I. V. Shadrivov, and D. A. Powell, Phys. Rev. Appl. **8**, 014019 (2017).
110 H. Zhao, Z. Chen, R. Zhao, and L. Feng, Nat. Commun. **9**, 1764 (2018).
111 S. H. G. Chang, and C. Y. Sun, Opt. Express **24**, 16822 (2016).
112 X. Gu, R. Bai, C. Zhang, X. R. Jin, Y. Q. Zhang, S. Zhang, and Y. P. Lee, Opt. Express **25**, 11778 (2017).
113 H. Yin, R. Bai, X. Gu, C. Zhang, G. R. Gu, Y. Q. Zhang, X. R. Jin, and Y. P. Lee, Opt. Commun. **414**, 172 (2018).
114 D. Frese, Q. Wei, Y. Wang, L. Huang, and T. Zentgraf, Nano Lett. **19**, 3976 (2019).
115 Z. Li, W. Liu, H. Cheng, J. Liu, S. Chen, and J. Tian, Sci. Rep. **6**, 35485 (2016).
116 T. Cai, G. M. Wang, S. W. Tang, H. X. Xu, J. W. Duan, H. J. Guo, F. X. Guan, S. L. Sun, Q. He, and L. Zhou, Phys. Rev. Appl. **8**, 034033 (2017).
117 W. Pan, T. Cai, S. Tang, L. Zhou, and J. Dong, Opt. Express **26**, 17447 (2018).
118 Y. Jing, Y. Li, J. Zhang, J. Wang, M. Feng, H. Ma, and S. Qu, Opt. Express **27**, 21520 (2019).
119 T. Cai, S. W. Tang, G. M. Wang, H. X. Xu, S. L. Sun, Q. He, and L. Zhou, Adv. Opt. Mater. **5**, 1600506 (2017).
120 T. Cai, G. M. Wang, H. X. Xu, S. W. Tang, H. Li, J. G. Liang, and Y. Q. Zhuang, Annalen Der Phys. **530**, 1700321 (2018).
121 Y. Zhuang, G. Wang, T. Cai, and Q. Zhang, Opt. Express **26**, 3594 (2018).
122 K. Chen, G. Ding, G. Hu, Z. Jin, J. Zhao, Y. Feng, T. Jiang, A. Alù, and C. Qiu, Adv. Mater. **32**, 1906352 (2020).
123 B. Yang, T. Liu, H. Guo, S. Xiao, and L. Zhou, Sci. Bull. **64**, 823

(2019).
124 A. Forouzmand, and H. Mosallaei, ACS Photon. **5**, 1427 (2018).
125 H. Xu, G. Hu, M. Jiang, S. Tang, Y. Wang, C. Wang, Y. Huang, X. Ling, H. Liu, and J. Zhou, Adv. Mater. Technol. **5**, 1900710 (2020).
126 Y. Zhou, I. I. Kravchenko, H. Wang, H. Zheng, G. Gu, and J. Valentine, Light Sci. Appl. **8**, 80 (2019).
127 A. Arbabi, E. Arbabi, Y. Horie, S. M. Kamali, and A. Faraon, Nat. Photon. **11**, 415 (2017).
128 H. Kwon, E. Arbabi, S. M. Kamali, M. S. Faraji-Dana, and A. Faraon, Nat. Photon. **14**, 109 (2020).
129 Z. Wu, Y. Ra'di, and A. Grbic, Phys. Rev. X **9**, 011036 (2019).
130 W. Ma, F. Cheng, and Y. Liu, ACS Nano **12**, 6326 (2018).
131 Z. Liu, D. Zhu, S. P. Rodrigues, K. T. Lee, and W. Cai, Nano Lett. **18**, 6570 (2018).
132 Y. Li, Y. Xu, M. Jiang, B. Li, T. Han, C. Chi, F. Lin, B. Shen, X. Zhu, L. Lai, and Z. Fang, Phys. Rev. Lett. **123**, 213902 (2019).
133 Z. Wu, M. Zhou, E. Khoram, B. Liu, and Z. Yu, Photon. Res. **8**, 46 (2020).